Electronic Supplementary Material (ESI)

Co-doped Ni-Mo oxides: Highly efficient and robust electrocatalyst for urea electrooxidation assisted hydrogen production

Xiangyun Liu,[a, b] Hehe Qin,[a, b] Genxiang Wang,[c] Qiuju Li,[a, b] Qisu Huang,[a, b] Zhenhai Wen,[c] Shun Mao*[a, b]

[a] Cllege of Environmental Science and Engineering, Biomedical Multidisciplinary Innovation Research Institute, Shanghai East Hospital, State Key Laboratory of Pollution Control and Resource Reuse, Tongji University, 1239 Siping Road, Shanghai 200092, China. E-mail: shunmao@tongji.edu.cn

[b] Shanghai Institute of Pollution Control and Ecological Security, Shanghai 200092, China

[c] CAS Key Laboratory of Design and Assembly of Functional Nanostructures, Fujian Provincial Key Laboratory of Nanomaterials, Fujian Institute of Research on the Structure of Matter, Chinese Academy of Sciences, Fuzhou 350002, China

Text S1. Characterizations

Field-emission scanning electron microscope (SEM, SU8010) was used to study the morphology and structure of the catalyst. The transmission electron microscopy (TEM) and high-resolution TEM (HRTEM) images were obtained on a FEITecnai G2 F30 microscope with energy-diffusive X-ray spectroscopy (EDS) attachment. X-ray photoelectron spectroscopy (XPS) results were obtained by PHI Quantera SXMTM Scanning X-ray Microprobe TM at 20 kV. X-ray diffraction (XRD) patterns were recorded on a Bruker D8 Advance X-ray diffractometer. The inductivity coupled plasma-optical emission spectroscopy (ICP-OES) was used to measure the Ni/Co ratio of the catalyst. The ion chromatography (IC) and ultraviolet spectrophotometer (UV-Vis) spectra were used to study the electrolysis products.

Text S2. Determination of urea

The urea was spectrophotometrically determined by the diacetylmonoxime method [1] . First, 100 μl aliquot of the solution was removed from the electrolysis cell and diluted to 1 ml. Then, 0.2 ml diluted solution, 2 ml acid-ferric solution (10 ml concentrated phosphoric acid, 30 ml concentrated sulfuric acid, 60 ml deionized water, and 16.67 mg ferric chloride hexahydrate), 1 ml diacetylmonoxime (DAMO)-thiosemicarbazide (TSC) solution (0.5 g DAMO and 10 mg TSC were dissolved in 100 ml deionized water), and 4.8 ml H_2O were mixed. The solution was heated in water bath at 100℃ for 20 minutes. After cooling to room temperature, the absorbance was measured at 525 nm using a UV–Vis spectrophotometer (Shimadzu UV-2700). The concentration–absorbance calibration curve was obtained using standard urea solution (**Fig. S7a**), which contained the same concentrations of electrolytes as used in the electrocatalysis experiments.

Text S3. Determination of nitrite (NO_2^-) and nitrate (NO_3^-)

The amounts of NO_2^- and NO_3^- were measured by an ion chromatogram instrument (ICS-2000). The corresponding calibration curves of NO_2^- and NO_3^- are shown in **Fig. S7b-c**.

Text S4. Energy consumption analysis

The energy consumption (kWh kg^{-1} H_2) was estimated according to the following equation:

$$\text{Energy consumption (kWh kg}^{-1}\text{ H}_2) = U \times I \times t = U \times I \times \frac{n(H_2) \times 2F}{I} = n(H_2) \times 2F \times U$$

where U (V), I (A), n (H_2) (mol), F (C/mol), and t (s) is the working potential, the current, the amount of hydrogen, faraday constant (96485 C/mol), and reaction time, respectively.

Text S5. Density functional theory (DFT) simulation

The plane-wave code Vienna ab-initio simulation package (VASP) program was used to perform all the spin-polarized density functional theory (DFT) calculations within the generalized gradient approximation (GGA) using the Perdew-Burke-Ernzerhof (PBE) formulation [2], [3], [4]. The projected augmented wave (PAW) potentials were chosen to describe the ionic cores and take valence electrons into account using a plane-wave basis set with a kinetic energy cutoff of 500 eV [5], [6]. The valence electron configurations applied in this work include $5s^1 4d^5$(Mo), $4s^2 3d^7$(Co), $4s^2 3d^8$(Ni), $2s^2 2p^2$ (C), $2s^2 2p^3$ (N), $2s^2 2p^4$ (O), and $1s^1$(H). Partial occupancies of the Kohn−Sham orbitals were allowed using the Gaussian smearing method with a width of 0.02 eV [7]. The electronic energy was considered self-consistent when the energy change was smaller than 10^{-6} eV.

The equilibrium lattice constants of [$NiMoO_4$] unit cell was optimized when using a 4×4×5 Monkhorst-Pack k-point grid for Brillouin zone sampling with a = 9.916, b = 8.802, and c = 7.400 Å. These lattice constants were used to build the $NiMoO_4$ (2 2 -2) surface slab with 5

atomic layers, which contains 24 Ni atoms, 16 Mo atoms, and 72 O atoms. These surfaces mentioned above were chosen since these surfaces were identified by HRTEM images. The Co atom was put in the $NiMoO_4$ model to consider the effect of doped Co. This slab was separated by a 15 Å vacuum layer in the z-direction between the slab and its periodic images. During structural optimizations of the (2 2 -2) surface model, a 3×3×1 gamma-point centered k-point grid for the Brillouin zone was used. All the atomic layers were allowed to fully relax.

The adsorption energy (E_{ads}) of an adsorbate (A) was defined as:

$E_{ads} = E_{A/surf} - E_{surf} - E_A$,

where $E_{A/surf}$, E_{surf}, and E_A is the energy of A adsorbed on the surface slab, the energy of surface slab, and the energy of adsorbate, respectively.

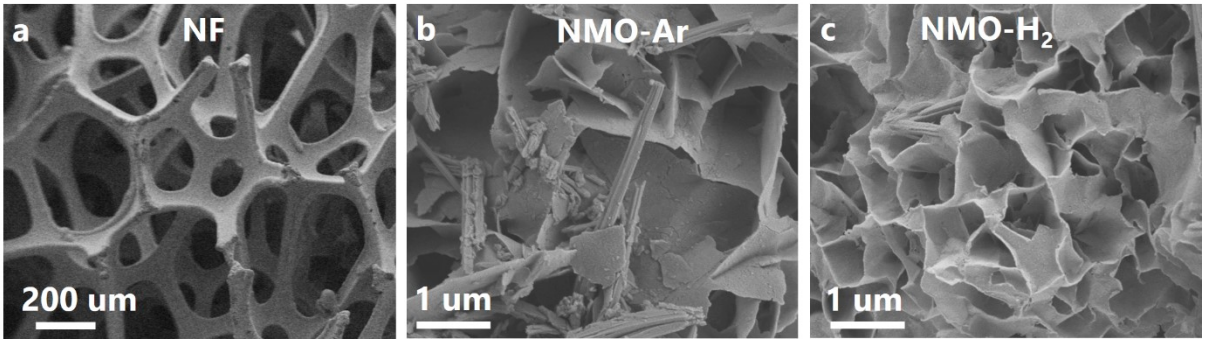

Figure S1. SEM images of (a) NF, (b) NMO-Ar, and (c) NMO-H_2.

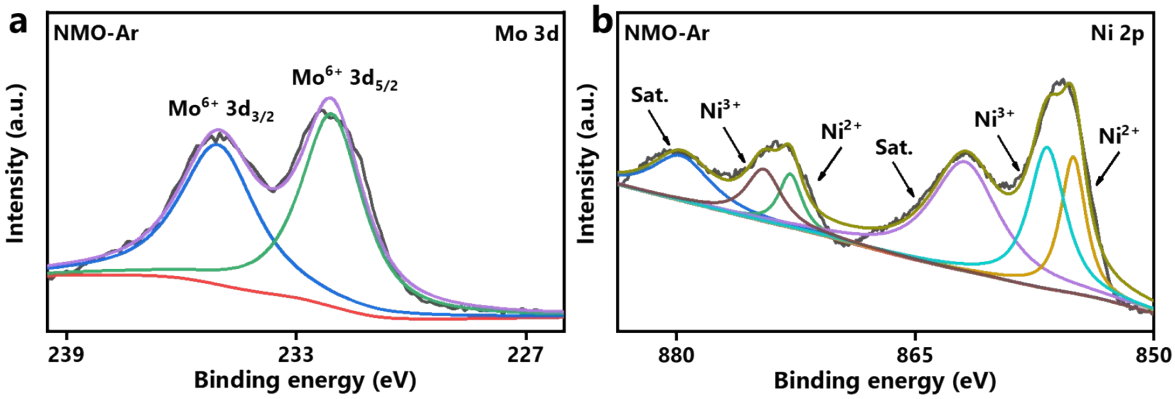

Figure S2. XPS spectra of Mo 3d and Ni 2p in NMO-Ar.

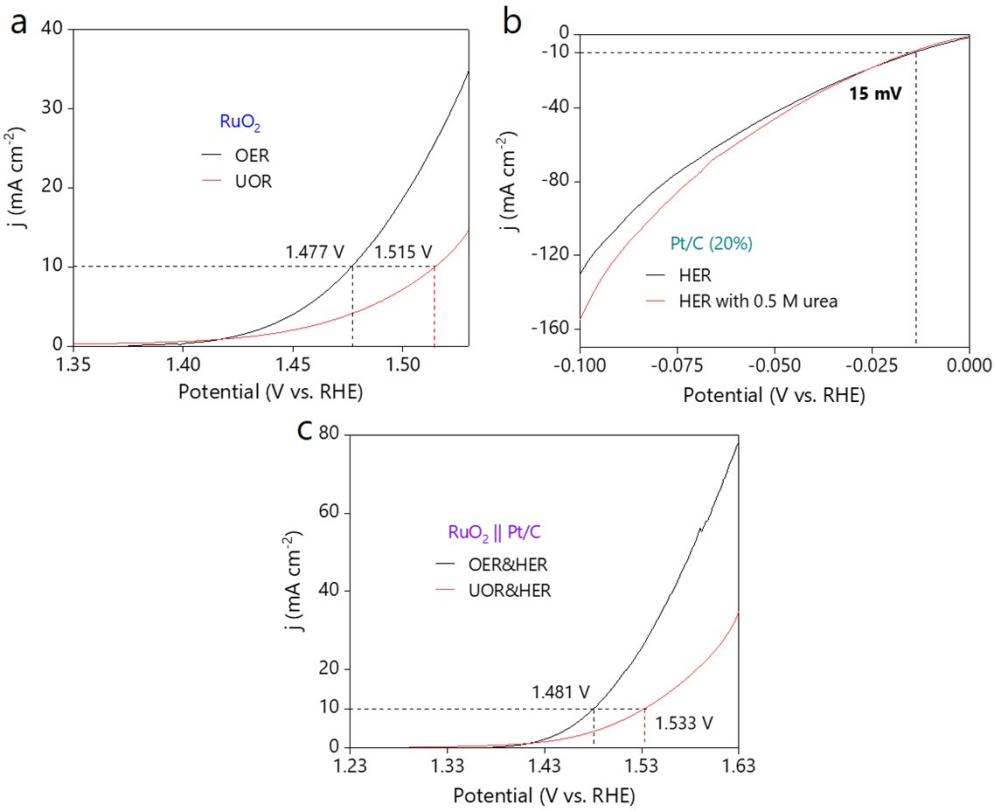

Figure S3. (a) Polarization curves of RuO_2 for UOR and OER in 1 M KOH without and with 0.5 M urea. (b) Polarization curves of Pt/C(20%) for HER in 1 M KOH without and with 0.5 M urea. (c) Polarization curves of RuO_2 ‖ Pt/C(20%) for water electrolysis and urea electrolysis. Scan rate: 2 mV s^{-1}.

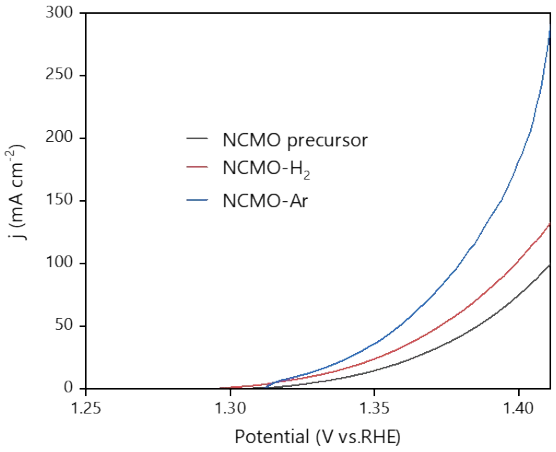

Figure S4. Comparison of the UOR activities of the NCMO precursor, NCMO-H_2, and NCMO-Ar. Scan rate: 2 mV s^{-1}.

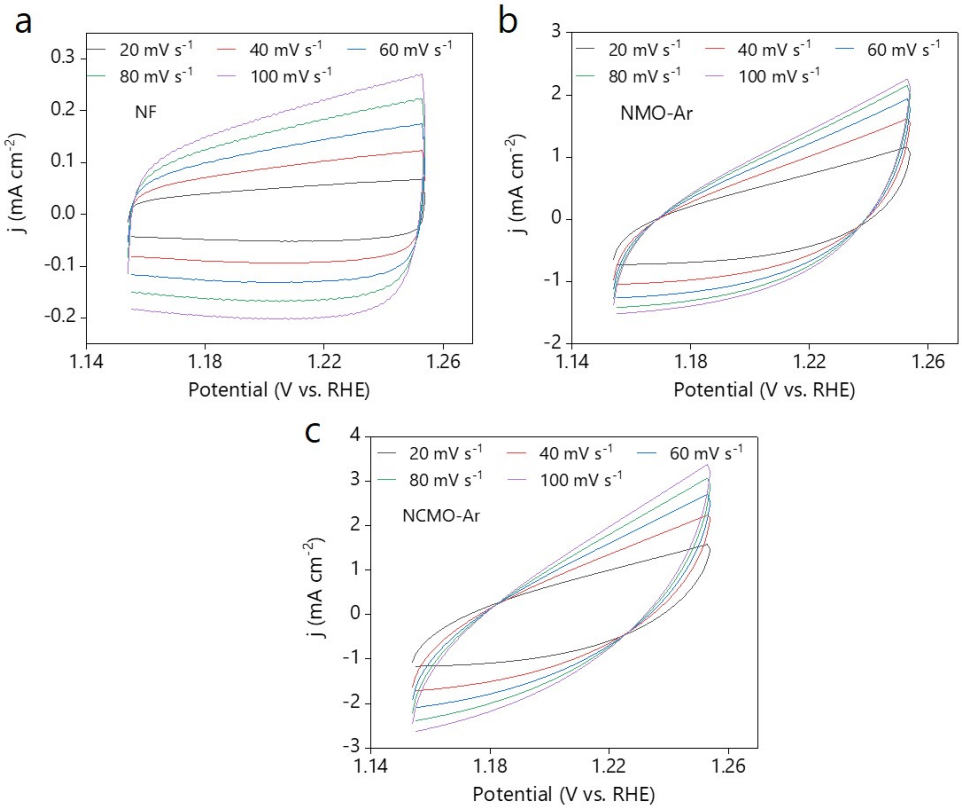

Figure S5. CV plots of (a) NF, (b) NMO-Ar, and (c) NCMO-Ar in 1 M KOH with 0.5 M urea at different scan rates from 1.154 V to 1.254 V.

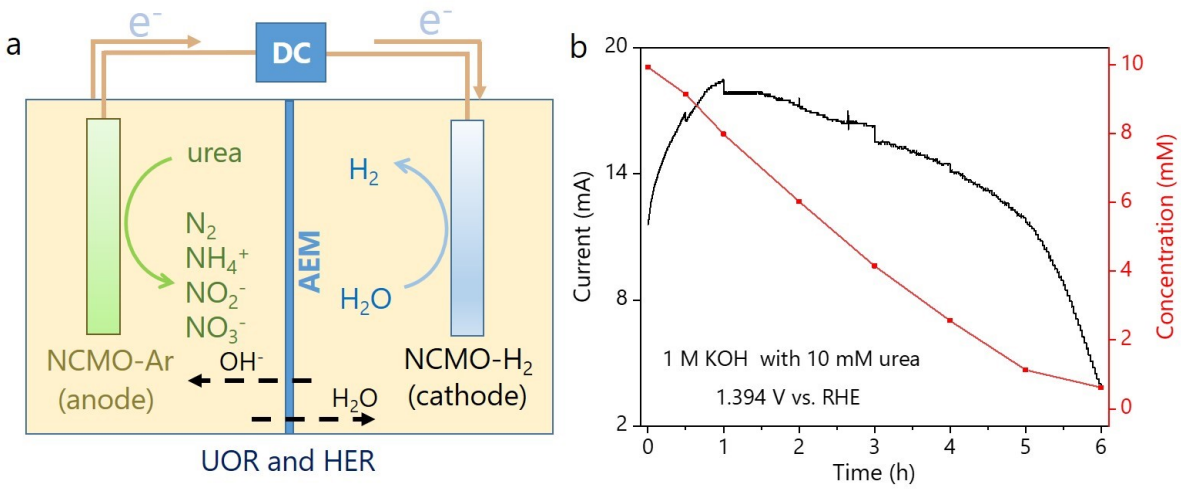

Figure S6. Urea oxidation in the NCMO-Ar anodic system at 1.394 V without iR correction. (a) Schematic of dual-chamber electrolysis cell with the anion exchange membrane (AEM). (b) The evolutions of anodic current and urea concentration during the 6 hr test in 1 M KOH with 10 mM urea.

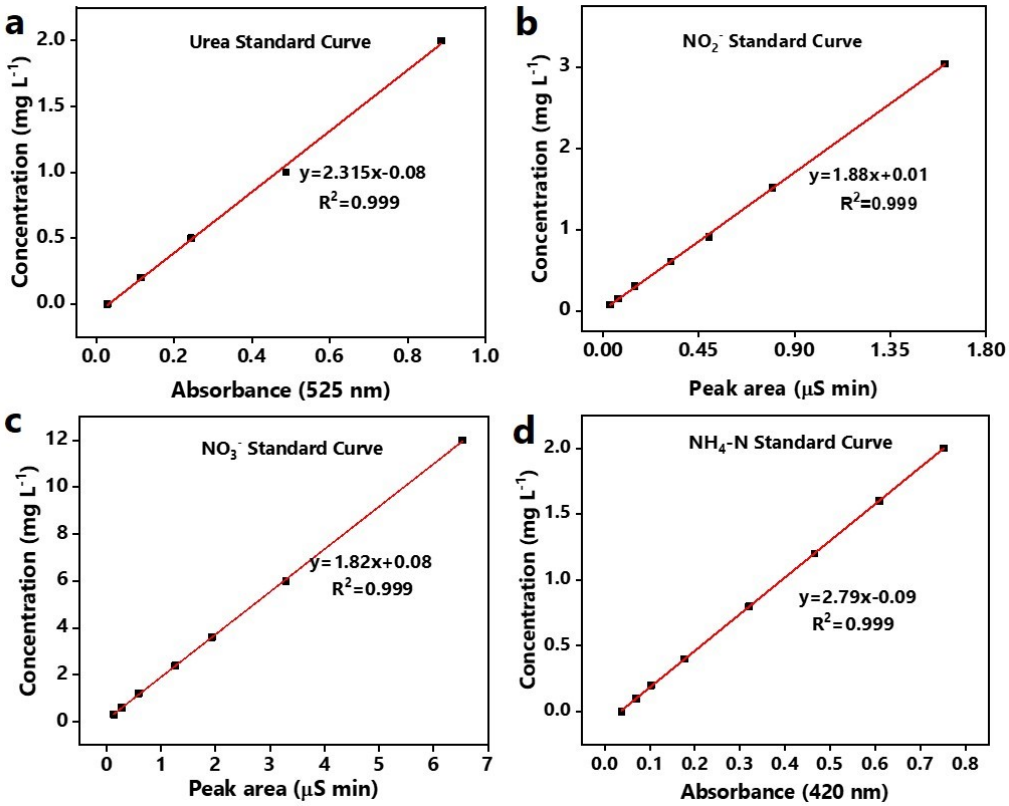

Figure S7. Calibration curves for (a) urea measurement by UV-VIS (TU-1901), (b) NO_2^- and (c) NO_3^- measurement by IC, and (d) NH_4-N measurement by UV-VIS (T6).

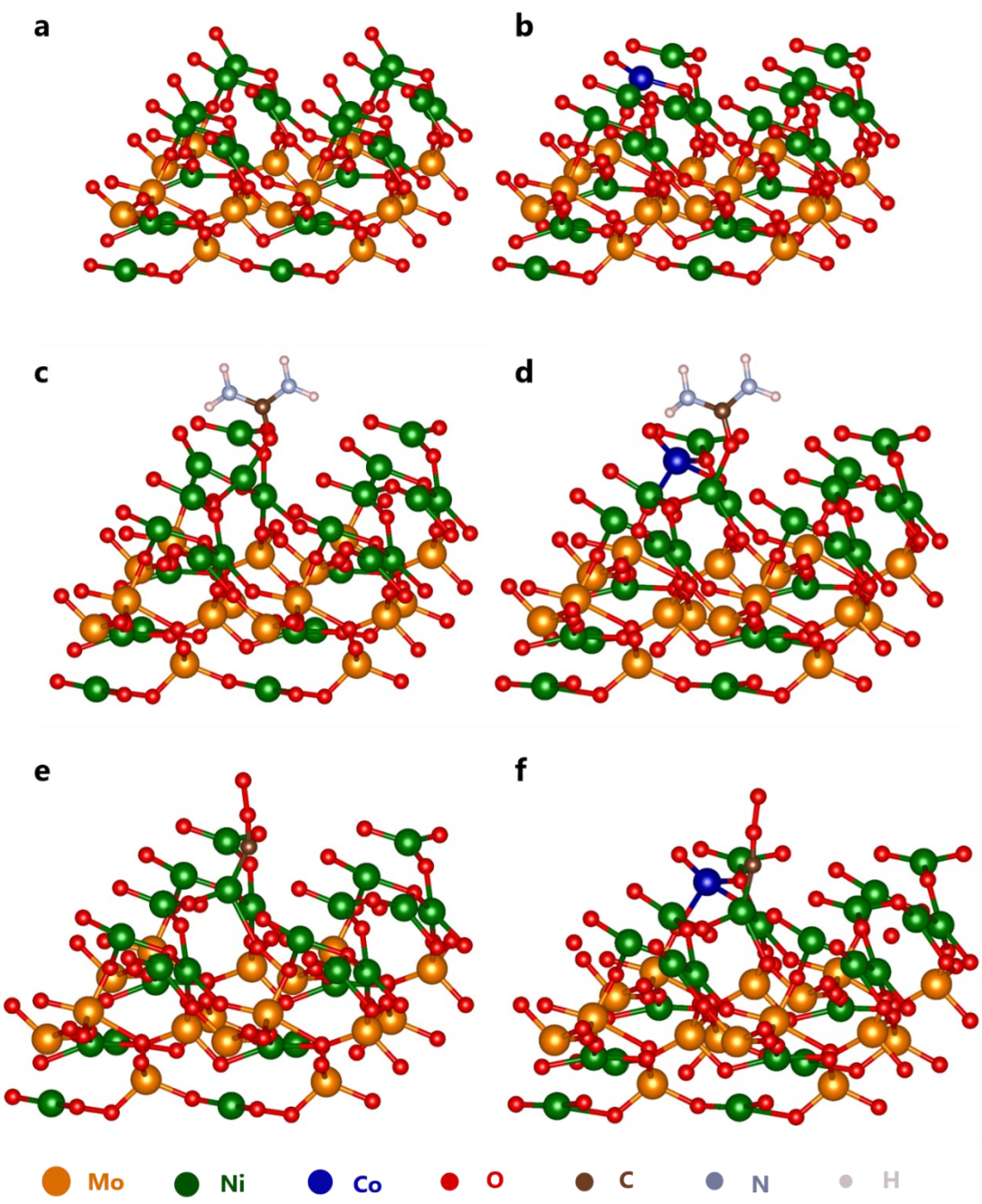

Figure S8. Optimized structures of (a) NMO-Ar, (b) NCMO-Ar, (c) NMO-Ar-urea*, (d) NCMO-Ar-urea*, (e) NMO-Ar-*COO, and (f) NCMO-Ar-*COO in DFT simulation. The blue, green, orange, brownness, silver, red, and light pink sphere represents the Co, Ni, Mo, C, N, O, and H atom, respectively.

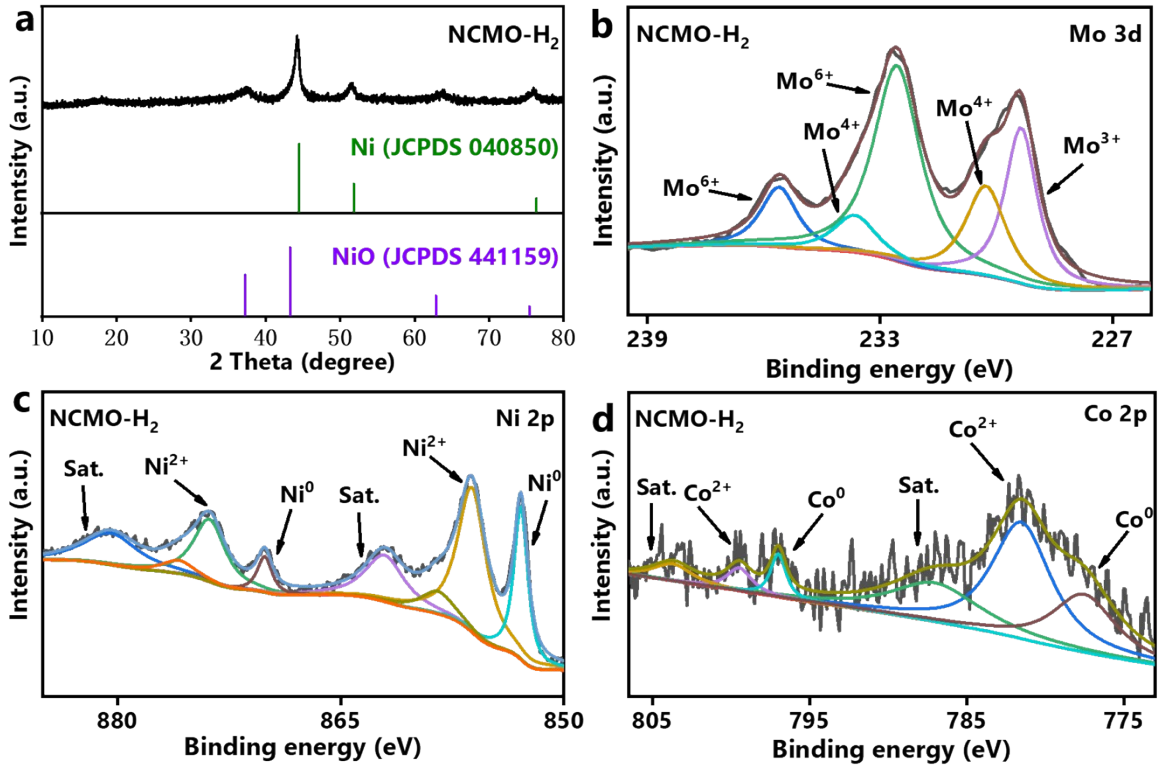

Figure S9. (a) XRD patterns of NCMO-H_2. (b-d) XPS spectra of Mo 3d, Ni 2p, and Co 2p in NCMO-H_2.

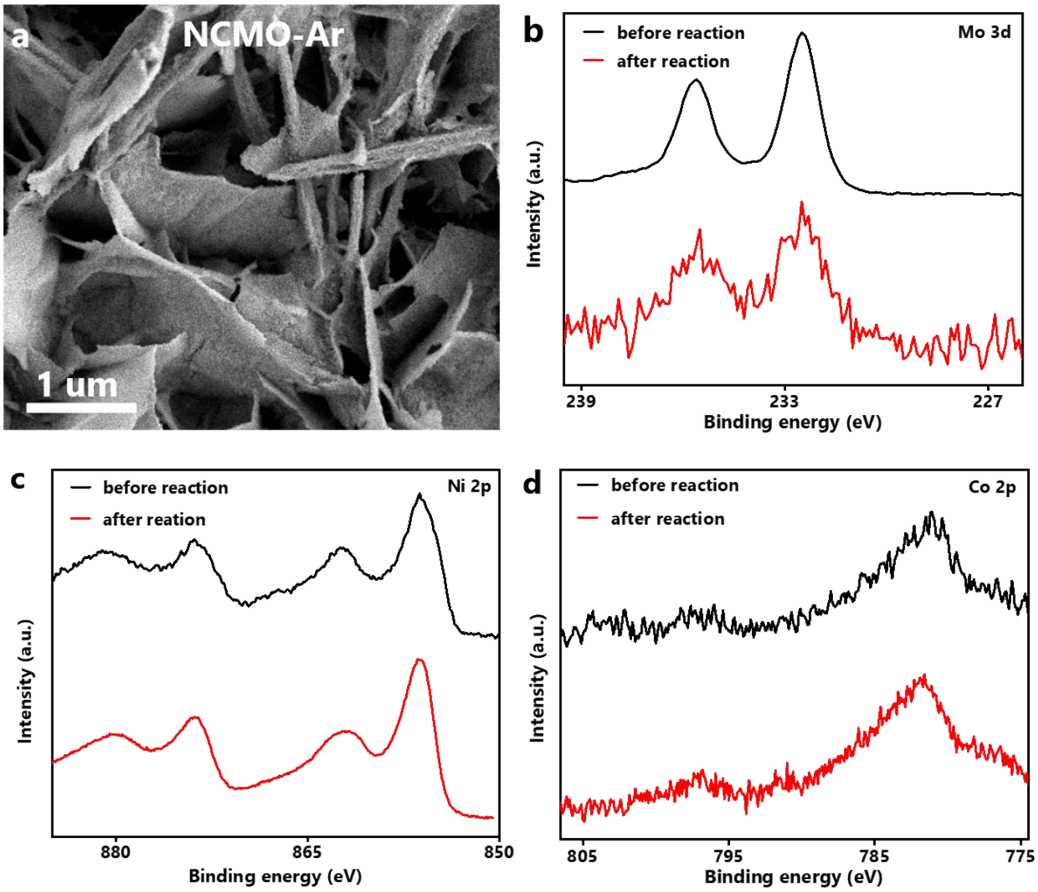

Figure S10. SEM image of (a) NCMO-Ar after 200 h electrolysis at 100 mA cm^{-2}. XPS spectra of (b) Mo 3d, (c) Ni 2p, and (d) Co 2p of NCMO-Ar before and after 200 h electrolysis at 100 mA cm^{-2}.

Table S1. The Ni and Co contents in NCMO-Ar and NCMO-H_2.

Catalyst	Content (at.%)	
	Ni	Co
NCMO-Ar	49.60	1.83
NCMO-H_2	69.01	1.71

Table S2. Comparison of the UOR activity of NCMO-Ar with representative Ni-based catalysts.

Catalyst	Electrolyte	Scan rate ($mV\ s^{-1}$)	Potential (mV)	Ref.
NCMO-Ar	**1 M KOH + 0.5 M urea**	**2**	**1.324 @ 10 mA cm^{-2}** **1.38 @ 100 mA cm^{-2}** **1.404 @ 200 mA cm^{-2}**	**This work**
NF/NiMoO-Ar	1 M KOH + 0.5 M urea	2	1.37 @ 10 mA cm^{-2}	*Energy Environ. Sci.* **2018**, *11*, 1890.[8]
r-$NiMoO_4$/NF	1 M KOH + 0.5 M urea	5	1.60 V @ 249.5 mA cm^{-2}	*ACS Catal.* **2018**, *8*, 1.[9]
Ni-WOx	1 M KOH + 0.33 M urea	10	1.4 @ 100 mA cm^{-2}	*Angew. Chem. Int. Ed.* **2021**, *60*, 10577.[10]
NiClO-D	1 M KOH + 0.33 M urea	5	1.60 V @ 264 mA cm^{-2}	*Angew. Chem. Int. Ed.* **2019**, *58*, 16820.[11]
NCVS	1 M KOH + 0.33 M urea	5	1.35 @ 10 mA cm^{-2}	*ACS Catal.* **2021**, *12*, 569.[12]
Ni_2P/MoO_2/NF	1 M KOH + 0.5 M urea	2	1.35 @ 10 mA cm^{-2}	*Appl. Catal. B* **2020**, *269*, *118803*.[13]
Ni-MOF	1 M KOH + 0.5 M urea	5	1.381 @ 10 mA cm^{-2}	*Chem. Eng. J.* **2020**, *395*, 125166.[14]

NF: nickel foam
r-$NiMoO_4$: oxygen-vacancy-rich $NiMoO_4$
NiClO-D: NiClOH derived catalyst
NCVS: Co, V co-doped NiS_2

Table S3. Comparison of the HER activity of NCMO-H_2 with representative HER catalysts.

Catalyst	Electrolyte	Scan rate ($mV\ s^{-1}$)	Potential (mV)	Ref.
NCMO-H_2	**1 M KOH + 0.5 M urea**	**2**	**26 @ 10 mA cm^{-2}** **85 @ 100 mA cm^{-2}**	**This work**
$Co_2Mo_3O_8$	1 M KOH + 0.5 M urea	1	37 @ 10 mA cm^{-2} 140 @ 100 mA cm^{-2}	*Nano Energy* **2021**, *87*, 106217.[15]
Rh_{SA}-S-Co_3O_4	1 M KOH + 0.5 M urea	2	45 @ 10 mA cm^{-2}	*Energy Environ. Sci.* **2021**, *14*, 6494.[16]
Ru-Co_2P/N-C/NF	1 M KOH + 0.5 M urea	5	65 @ 10 mA cm^{-2}	*Chem. Eng. J.* **2021**, *408*, 127308.[17]
Ni-Mo nanotube	1 M KOH + 0.1 M urea	5	44 @ 10 mA cm^{-2}	*Nano Energy* **2019**, *60*, 894.[18]
$Ni_{1.6}Co_{0.4}P$/C@HCNs	1 M KOH + 0.33 M urea	5	145 @ 10 mA cm^{-2}	*Nanoscale* **2020**, *12*, 16123.[19]
MnO_2/$MnCo_2O_4$/Ni	1 M KOH + 0.5 M urea	5	200 @ 10 mA cm^{-2}	*J. Mater. Chem. A* **2017**, *5*, 7825.[20]

NF: nickel foam
Rh_{SA}-S-Co_3O_4: Rh single-atom-strain on the surface of a Co_3O_4
HCNs: hollow carbon nanospheres

Table S4. Performance comparison of representative urea electrolysis systems.

Catalyst	Electrolyte	Voltage (V) @ 10 mA cm^{-2}	Stability	Ref.
NCMO-Ar || NCMO-H_2	**1 M KOH + 0.5 M urea**	**1.342 V**	**200 h @ 100 mA cm^{-2}**	**This work**
Rh_{SA}-S-Co_3O_4	1 M KOH + 0.5 M urea	1.33 V	100 h @ 100 mA cm^{-2}	*Energy Environ. Sci.* **2021**, *14*, 6494.[16]
P-Mo-$Ni(OH)_2$	1 M KOH + 0.1 M urea	1.36 V	80 h @ 1.80 V	*Appl. Catal. B* **2020**, *260*, 118154.[21]
P-$CoNi_2S_4$	1 M KOH + 1 M urea	1.402 V	100 h @ 10 mA cm^{-2}	*Angew. Chem. Int. Ed.* **2021**, *60*, 22885.[22]
$Ni_2Fe(CN)_6$	1 M KOH + 0.5 M urea	1.38 V	1 h @ different voltage	*Nat. Energy* **2021**, *6*, 904.[23]
O-NiMoP/NF	1 M KOH + 0.5 M urea	1.36 V	10 h @ 20 mA cm^{-2}	*Adv. Funct. Mater.* **2021**, *31*, 2104951.[24]
CoMn/$CoMn_2O_4$	1 M KOH + 0.5 M urea	1.51 V	16.67 h @ 1.68 V	*Adv. Funct. Mater.* **2020**, *30*, 2000556.[25]
Ni@NCNT	1 M KOH + 0.5 M urea	1.56 V	10 h @ 10 mA cm^{-2}	*Appl. Catal. B* **2021**, *280*, 119436.[26]

NF: nickel foam
Rh_{SA}-S-Co_3O_4: Rh single-atom-strain on the surface of a Co_3O_4
P-Mo-$Ni(OH)_2$: plasma-activated Mo-$Ni(OH)_2$
P-$CoNi_2S_4$: phosphorized $CoNi_2S_4$
O-NiMoP: oxygen-incorporated NiMoP
NCNT: nitrogen-doped carbon nanotubes

REFERENCES

[1] C. Lv, L. Zhong, H. Liu, Z. Fang, C. Yan, M. Chen, Y. Kong, C. Lee, D. Liu, S. Li, J. Liu, S. Li, G. Chen, Q. Yan, G. Yu, *Nat. Sustain.* **2021**, 4, 868.

[2] G. Kresse, J. Furthmüller, *Comput. Mater. Sci.* **1996**, 6, 15.

[3] G. Kresse, J. Furthmuller, *Phys. Rev. B* **1996**, 54, 11169.

[4] J. P. Perdew, K. Burke, M. Ernzerhof, *Phys. Rev. Lett.* **1996**, 77, 3865.

[5] G. Kresse, D. Joubert, *Phys. Rev. B* **1999**, 59, 1758.

[6] P. E. Blochl, *Phys. Rev. B* **1994**, 50, 17953.

[7] S. Grimme, J. Antony, S. Ehrlich, H. Krieg, *J. Chem. Phys.* **2010**, 132, 154104 154104.

[8] Z. Y. Yu, C. C. Lang, M. R. Gao, Y. Chen, Q. Q. Fu, Y. Duan, S. H. Yu, *Energy Environ. Sci.* **2018**, 11, 1890.

[9] Y. Tong, P. Chen, M. Zhang, T. Zhou, L. Zhang, W. Chu, C. Wu, Y. Xie, *ACS Catal.* **2018**, 8, 1.

[10] B. Zhang, L. Wang, Y. Zhu, Y. Wen, S. Li, C. Cui, F. Ni, Y. Liu, H. Lin, Y. Li, H. Peng, *Angew. Chem. Int. Ed.* **2021**, 60, 10577.

[11] L. Zhang, L. Wang, H. Lin, Y. Liu, J. Ye, Y. Wen, A. Chen, L. Wang, F. Ni, Z. Zhou, S. Sun, Y. Li, B. Zhang, H. Peng, *Angew. Chem. Int. Ed.* **2019**, 58, 16820.

[12] Z. Ji, Y. Song, S. Zhao, Y. Li, J. Liu, W. Hu, *ACS Catal.* **2021**, 12, 569.

[13] M. Yang, Y. Jiang, M. Qu, Y. Qin, Y. Wang, W. Shen, R. He, W. Su, M. Li, *Appl. Catal. B* **2020**, 269, 118803.

[14] S. S. Zheng, Y. Zheng, H. G. Xue, H. Pang, *Chem. Eng. J.* **2020**, 395, 125166, 125166.

[15] K. Zhang, C. Liu, N. Graham, G. Zhang, W. Yu, *Nano Energy* **2021**, 87, 106217, 106217.

[16] A. Kumar, X. Liu, J. Lee, B. Debnath, A. R. Jadhav, X. Shao, V. Q. Bui, Y. Hwang, Y. Liu, M. G. Kim, H. Lee, *Energy Environ. Sci.* **2021**, 14, 6494.

[17] Y. Xu, T. Ren, K. Ren, S. Yu, M. Liu, Z. Wang, X. Li, L. Wang, H. Wang, *Chem. Eng. J.* **2021**, 408, 127308, 127308.

[18] J.-Y. Zhang, T. He, M. Wang, R. Qi, Y. Yan, Z. Dong, H. Liu, H. Wang, B. Y. Xia, *Nano Energy* **2019**, 60, 894.

[19] S. Rezaee, S. Shahrokhian, *Nanoscale* **2020**, 12, 16123.

[20] C. Xiao, S. Li, X. Zhang, D. R. MacFarlane, *J. Mater. Chem. A* **2017**, 5, 7825.

[21] W. Zhang, Y. Tang, L. Yu, X.-Y. Yu, *Appl. Catal. B* **2020**, 260, 118154, 118154.

[22] X.-W. D. Lou, *Angew. Chem. Int. Ed.* **2021**, 60, 22885.

[23] S.-K. Geng, Y. Zheng, S.-Q. Li, H. Su, X. Zhao, J. Hu, H.-B. Shu, M. Jaroniec, P. Chen, Q.-H. Liu, S.-Z. Qiao, *Nat. Energy* **2021**, 6, 904.

[24] H. Jiang, M. Sun, S. Wu, B. Huang, C.-S. Lee, W. Zhang, *Adv. Funct. Mater.* **2021**, 31, 2104951.

[25] C. Wang, H. Lu, Z. Mao, C. Yan, G. Shen, X. Wang, *Adv. Funct. Mater.* **2020**, 30, 2000556.

[26] Q. Zhang, F. M. D. Kazim, S. Ma, K. Qu, M. Li, Y. Wang, H. Hu, W. Cai, Z. Yang, *Appl. Catal. B* **2021**, 280, 119436.